Atmospheric Environment 267 (2021) 118775

Contents lists available at ScienceDirect

Atmospheric Environment

journal homepage: www.elsevier.com/locate/atmosenv

Impact of different urban canopy models on air quality simulation in Chengdu, southwestern China

Haofan Wang, Zhihong Liu, Yang Zhang *, Zhengyang Yu, Chunrong Chen

College of Resources and Environment, Chengdu University of Information Technology, Chengdu, 610225, China

HIGHLIGHTS

1. The feasibility of different urban canopy models in complex terrain is investigated over the megacity Chengdu.
2. Overestimation of wind speed under weak wind fields has been improved by employing urban canopy models.
3. The extensive use of air conditioning systems shows improvements in air quality over Chengdu in summer.

ARTICLE INFO

Keywords:
Urban canopy model
WRF-CMAQ
Chengdu
Air quality

ABSTRACT

Urban air pollution has emerged as a prominent public health concern in megacities and highly developed city clusters. Accurate modelling of urban air quality over complex terrain is challenging due to heterogeneous urban landscapes and multiscale land-atmosphere interactions. In this study, we investigated the applicability of urban canopy models in the Weather Research and Forecast (WRF) model and assessed the impacts of implementing these models on the urban air quality simulation in the Community Multiscale Air Quality (CMAQ) model over the megacity Chengdu, southwestern China. The land use and land cover of Chengdu were updated in WRF by using the land-use products in 2017 from the Moderate-resolution Imaging Spectroradiometer (MODIS). Sensitivity experiments with various urban canopy models were conducted to investigate the feasibility of different urban canopy models on WRF-CMAQ simulations. We found that the SLAB model significantly underestimates NO2 and PM2.5 concentrations, with mean fractional bias in winter (summer) reaching 52.93% (−50.34%) and −102.82% (−23.12%), respectively. Such large biases are mainly attributed to overpredicted wind speeds resulting from the flat structure in the SLAB model. In contrast, the BEM (a multilayer urban canopy model coupled with air-conditioning systems) model yields the best model performance in both winter and summer, with mean fractional errors of 33.15% (38.96%) and 34.10% (33.15%) for NO2 and PM2.5 in winter (summer), respectively. The UCM (a single-layer urban canopy model) model illustrates good performance in summer, with MFBs of 25.61% for NO2 and 19.03% for PM2.5, while NO2 and PM2.5 concentrations are overestimated in winter, with MFBs of 62.58% and 38.19%, respectively. In contrast, BEP (a multilevel urban canopy model)-modelled NO2 (MFB: 37.18%) and PM2.5 (MFB: 18.72%) correlate well with observations in winter, while significantly overestimated air pollutant concentrations in summer with MFBs of NO2 and PM2.5 of 49.70% and 44.50%, respectively. In general, the BEP model and the BEM model are well suited for air quality simulations over Chengdu in winter, and the BEM model could be considered for air quality simulations in summer. Furthermore, we assessed the effects of extensive usage of air conditioning systems in Chengdu during summertime, and the results suggest that using air conditioning systems facilitates the dispersion of air pollutants over Chengdu. This study pinpoints the limitations of default WRF configurations and tests the applicability of urban canopy models in the WRF-CMAQ model over Chengdu, in addition highlighting the crucial role of urban canopy models in urban meteorological-air quality simulations.

* Corresponding author.
E-mail address: zhangyang@cuit.edu.cn (Y. Zhang).

https://doi.org/10.1016/j.atmosenv.2021.118775
Received 17 April 2021; Received in revised form 7 September 2021; Accepted 12 September 2021
Available online 6 October 2021

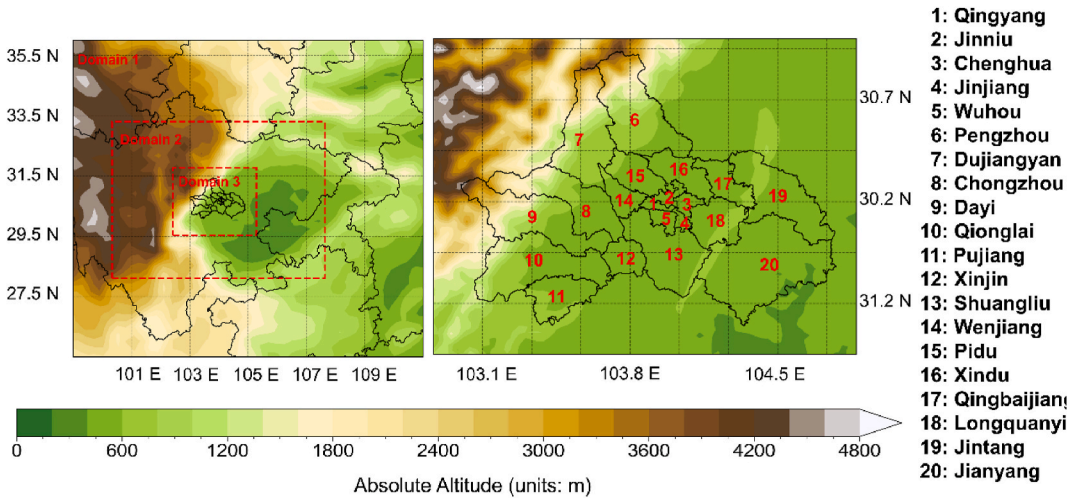

Fig. 1. Map of triple nested domains for the WRF-CMAQ model.

Table 1
WRF and CMAQ modelling configurations and inputs.

Model attribution	Configuration
Land use/cover data	Modify MODIS land cover data in 2017
Meteorological initial conditions (ICs) and boundary conditions (BCs)	NCEP Final (FNL) reanalysis data
Anthropogenic emissions	MEIC in 2017
Microphysics	Purdue Lin(Chen and Sun, 2002)
PBL physics scheme	MYJ (Janjić, 1994)
Shortwave and longwave radiation	Goddard (Chou et al., 2001) and Rapid Radiative Transfer Model (RRTM) (Mlawer et al., 1997)
Land surface model	Noah land surface model (LSM) (Ek et al., 2003)
Gas-phase chemistry	Carbon bond chemical reaction mechanism (CB06) (Yarwood et al., 2010)
Aerosol module	AERO6 (Pye et al., 2017; Murphy et al., 2017)

Note: MODIS = Moderate-resolution Imaging Spectroradiometer; NCEP = National Centers for Environmental Prediction; MEIC = Multiresolution Emission Inventory for China.

Table 2
Settings of canopy parameters.

	SLAB	UCM	BEP	BEM
Canopy layer description	No canopy layer	Single-layer	Multilayer	Multilayer
Fixed anthropogenic heat	No	Yes	Yes	Yes
Other anthropogenic heat	No	No	No	Yes
Fraction of vegetation	No	Yes	Yes	Yes
PBL coupling scheme	MYJ	MYJ	MYJ	MYJ

Table 3
Model parameters for UCM and BEP (BEM).

Parameter	Unit	Value	UCM	BEP (BEM)
Building height	m	20	YES	Table 3
Building width	m	15	YES	Table 3
Width of the road	m	10	YES	Table 3
Urban fraction	Fraction	0.95	YES	YES
Roof albedo	Fraction	0.2	YES	YES
Wall albedo	Fraction	0.2	YES	YES
Pavement albedo	Fraction	0.2	YES	YES
Roof roughness length	m	0.15	YES	YES
Wall roughness length	m	0.05	YES	NO
Pavement roughness length	m	0.05	YES	YES

Table 4
Model parameters for only BEP and BEM.

Street direction (°C)	Width of the road (m)	Building width (m)
0.0	15.0	15.0
90.0	15.0	15.0
Building height (m)		**Percentage (%)**
15.0		10.0
20.0		25.0
25.0		40.0

Note: The target temperature of the air-conditioning system in the BEM model is 24 °C.

1. Introduction

With ongoing industrialization and rapid economic growth, global megacities and city clusters have witnessed a continued urbanization process with an expansion of urban regions and changing urban landscapes (Li et al., 2019; Memon et al., 2009; Wu et al., 2019; Yan et al., 2020). The acceleration of urbanization has led to rapid changes in surface land use, and high-rise buildings in megacities have formed urban canopies, which alter the urban surface energy balance and surface roughness. These changes significantly affect processes of land-atmosphere interactions in the urban region (Arnfield, 2003; Memon et al., 2009; Zhang et al., 2010; Wang et al., 2021a) and contribute to air pollution and regional climate change (Gu et al., 2021; Hu et al., 2021; Lin et al., 2008; Wu et al., 2020; Wu et al., 2021; Yang et al., 2020a; Zhang et al., 2008).

To resolve the intraurban spatial patterns of meteorological conditions and air pollutants, the Weather Research and Forecast (WRF)–Community Multiscale Air Quality (CMAQ) modelling system has been widely used in regional air quality studies (Ma et al., 2019; Yang et al. 2020b, 2021; Wang et al., 2021a). While the WRF model could capture the variability of meteorological conditions in the urban atmosphere, the most widely adopted configuration in the WRF model without urban canopy models has considerable limitations in reproducing urban canopy structures (Liao et al., 2014; Vahmani and Ban-Weiss, 2016). Specifically, the default configuration of the SLAB model in WRF simplifies the urban area into a plane with greater roughness and less reflectivity (Wang and Hu, 2020). However, the actual city is a three-dimensional space, and buildings and streets impact shortwave radiation

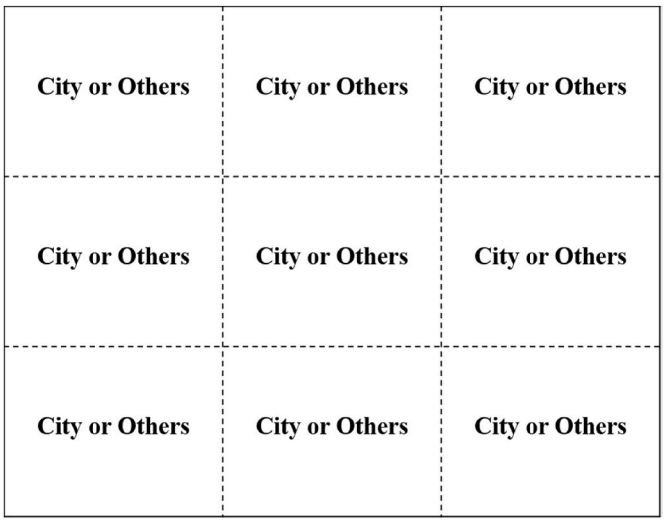

Fig. 2. Window diagram.

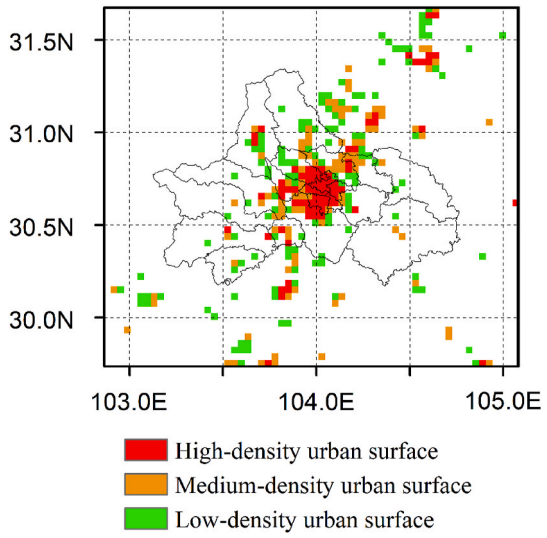

Fig. 3. Urban land cover types in Chengdu.

absorption, wind speed, and temperature in the city (Li et al., 2016). Therefore, it is challenging to accurately capture the complex physical and chemical processes within the city by using the SLAB model. In recent years, mesoscale numerical models coupled with urban canopies have been widely implemented to examine the dynamic thermal properties of the urban boundary layer (UBL) and deepen the understanding of local and regional climate change induced by urban canopies (Barlow, 2014). To represent the difference between the urban landscape and other land cover types, existing studies reconstructed the heat balance of the urban surface by changing the heat capacity and energy conductivity (Zhu et al., 2017). However, this method still has the limitation that the discrepancy of different urban structure forms could not reflect the heterogeneity of urban heat storage capacity (Salamanca et al., 2011). To adequately address this issue, three urban canopy models, including the single-layer urban canopy model (UCM), the multilayer canopy layer model (BEP), and the BEM (a multilayer urban canopy model coupled with air-conditioning systems) model, were developed and incorporated into the WRF model.

While rapid urbanization has occurred over global megacities and major city clusters, the impacts of the urbanization process on the urban environment are best illustrated at a local or regional scale given the complex multiscale interactions between topography, anthropogenic emissions, and meteorological conditions. In recent years, extensive studies have been carried out on mesoscale weather model systems coupled with urban canopies to explore their applicability to regional climate change and air quality. Liao et al. (2014) adopted canopy models with WRF to examine the applicability of the canopy model over the Yangtze River Delta (YRD) and found that implementing BEP and BEM models could improve the model performance in predicting 10-m wind speed over urban areas in contrast to the weak capability in the SLAB model, illustrating the necessity of incorporating urban canopy models towards optimizing urban meteorology-air quality simulations. Furthermore, Liao et al. (2015) adopted a canopy model to examine urban expansion over the YRD and recognized that human-induced urban expansion resulted in an increase in 2-m temperature and planetary boundary layer height (PBLH) while reducing 10-m wind speed, in turn leading to elevated O_3 levels and decreased PM_{10} concentrations. Similarly, Wang et al. (2009) utilized the WRF-UCM-Chem model to examine the expansion of urban regions over the Pearl River Delta (PRD) and YRD, and the results showed that both temperature and ambient O_3 concentrations increased due to the urbanization process. Most of the literature has focused on densely populated areas in eastern China (YRD, PRD, etc.), while there is limited work on the Sichuan Basin (SCB) (Wang et al., 2021b). Chengdu (Fig. 1), the typical megacity located in the SCB, is the most relevant and typical case due to its unique features of meteorological conditions and complex topography. Due to the rapid urbanization process and unique meteorological conditions, air pollution in Chengdu has become increasingly severe (Wu et al., 2021). Recent work has focused on understanding the causes of severe air pollution in Chengdu as well as the development of effective regulation

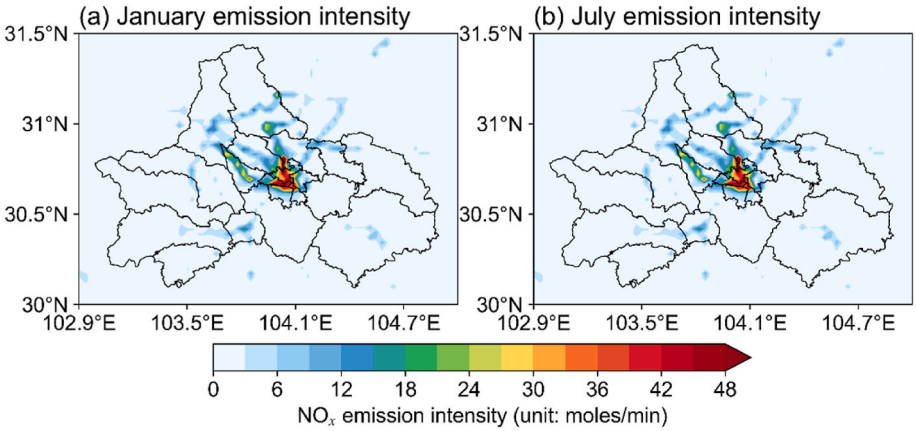

Fig. 4. Monthly average emission intensity of NO_x in (a) January and (b) July.

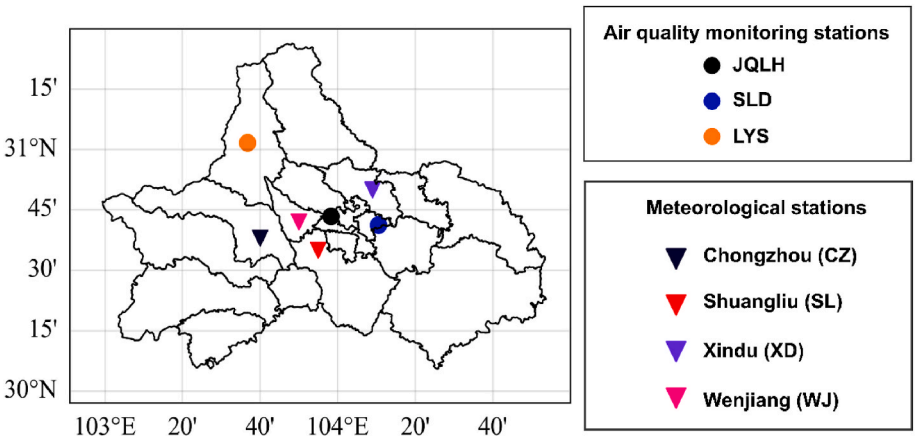

Fig. 5. The locations of meteorological measurements and air quality monitoring sites in Chengdu city.

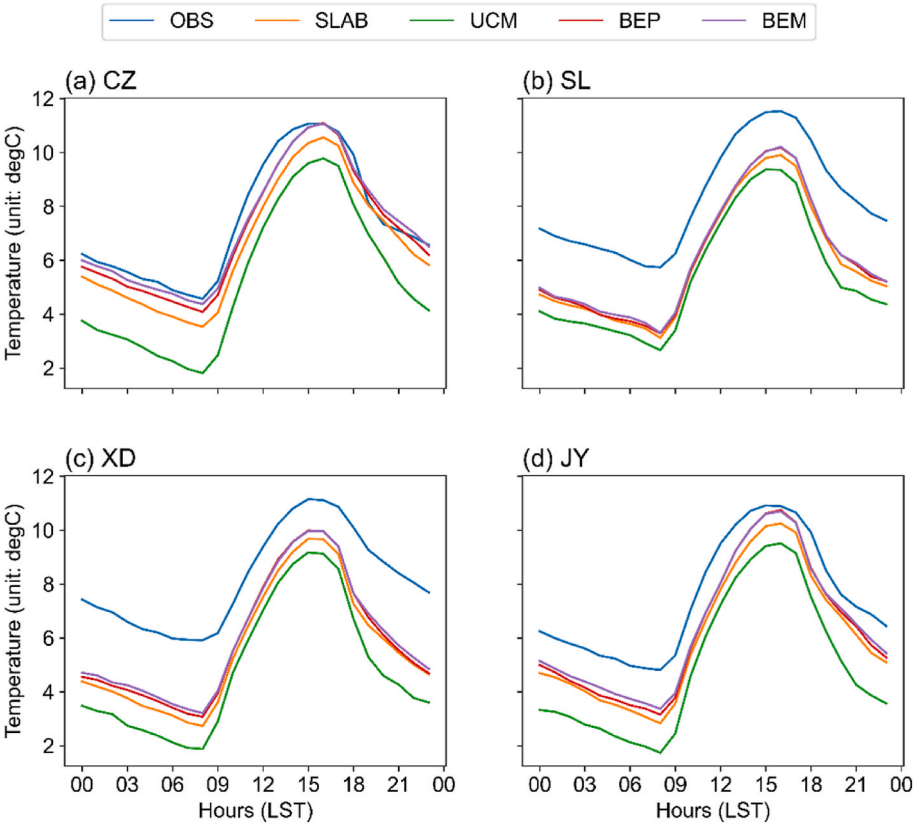

Fig. 6. Diurnal changes of 2-m temperature over Chengdu city in January.

policies (Yang et al. 2020a, 2021). However, previous meteorology-air quality modelling studies over Chengdu and the SCB often lack consideration of urban canopy structures, and the applicability of various urban canopy models has not yet been adequately assessed.

In this study, we tested the applicability of four urban canopy models (including SLAB (reference group), UCM, BEP, and BEM) in the WRF model and performed air quality simulations by using CMAQv5.3.2 to investigate the impact of urban canopy models on meteorological conditions and urban air quality over Chengdu city in summer and winter in 2017. In Section 2, we describe the observational data and configurations of the WRF-CMAQ model system. Section 3 presents the model evaluations against ground-level observations. In Section 4, we quantify the results of implementing urban canopy models on meteorological conditions and urban air quality. The conclusions are summarized in Section 5.

2. Data and methods

2.1. WRF–CMAQ model configurations

The WRF-CMAQ modelling system was utilized to simulate the meteorological conditions and air quality in this work (US EPA Office Of Research and Development, 2020). Meteorological conditions for driving the CMAQ model are provided by the Weather Research and Forecasting (WRFv4.1.2) model (Skamarock et al., 2019). Fig. 1 presents the triple nested domain, which is centred over Chengdu city. The horizontal resolution of each model domain is 27, 9, and 3 km. Each domain consists of 32 vertical layers from the ground to 100 hPa, with a

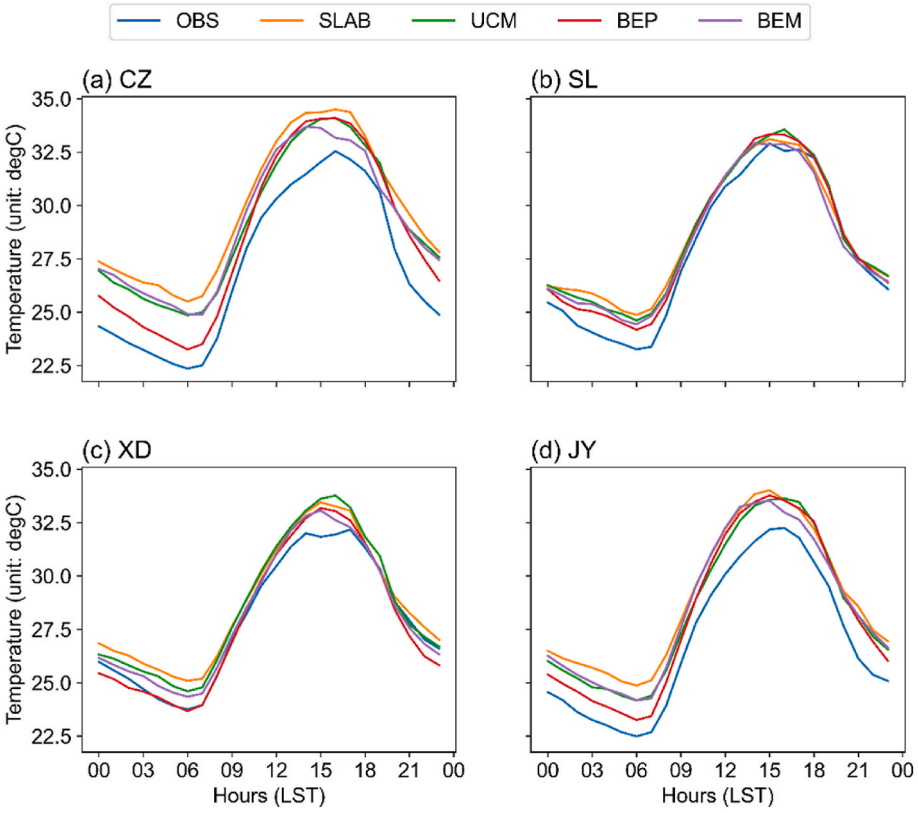

Fig. 7. Diurnal changes of 2-m temperature over Chengdu city in July.

Table 5
Statistical metrics of 2-m temperature under various urban canopy models.

Station name	Indicators	Mouth	SLAB	UCM	BEP	BEM
CZ	RMSE	Jan.	4.82	5.74	4.52	4.67
		July	7.05	5.77	5.01	6.02
	MB	Jan.	1.94	2.43	1.82	1.87
		July	3.04	2.36	1.93	2.51
	R	Jan.	0.74	0.73	0.75	0.73
		July	0.85	0.88	0.88	0.85
SL	RMSE	Jan.	6.16	6.89	5.98	5.88
		July	4.93	4.53	4.52	4.64
	MB	Jan.	2.61	2.99	2.54	2.49
		July	1.91	1.70	1.68	1.76
	R	Jan.	0.72	0.69	0.73	0.72
		July	0.81	0.85	0.84	0.83
XD	RMSE	Jan.	6.14	7.24	5.73	5.64
		July	4.96	4.82	4.68	4.76
	MB	Jan.	2.59	3.15	2.42	2.38
		July	1.86	1.80	1.75	1.74
	R	Jan.	0.74	0.69	0.76	0.76
		July	0.79	0.80	0.80	0.79
WJ	RMSE	Jan.	5.15	6.15	4.95	4.96
		July	6.13	5.07	4.95	5.52
	MB	Jan.	2.09	2.63	2.02	2.01
		July	2.48	1.94	1.88	2.13
	R	Jan.	0.74	0.70	0.74	0.73
		July	0.83	0.87	0.86	0.84
Overall result	RMSE	Jan.	4.94	6.23	6.19	5.30
		July	5.66	4.61	4.75	5.29
	MB	Jan.	2.02	2.66	2.63	2.19
		July	2.30	1.73	1.76	2.04
	R	Jan.	0.74	0.72	0.74	0.73
		July	0.87	0.83	0.79	0.85

Table 6
Statistical metrics for wind speed under different urban canopy models.

Overall results	SLAB	UCM	BEP	BEM
January MB	1.30	1.35	1.00	1.00
July MB	1.64	1.58	1.24	1.31

Table 7
Statistical metrics for CMAQ model evaluation over Chengdu in January 2017.

Station name	NO_2 in Jan.	SLAB	UCM	BEP	BEM
JQLH	MFB	−19.09%	97.70%	59.21%	53.59%
	MFE	41.53%	50.72%	32.76%	30.22%
	R	0.04	0.34	0.45	0.48
SLD	MFB	−114.68%	26.18%	−17.78%	−23.86%
	MFE	62.34%	38.32%	29.70%	28.94%
	R	−0.14	0.21	0.41	0.44
LYS	MFB	−25.02%	63.86%	70.11%	70.04%
	MFE	40.80%	38.14%	40.54%	40.30%
	R	0.14	0.24	0.21	0.23
Overall	MFB	−52.93%	62.58%	37.18%	33.26%
	MFE	48.22%	42.39%	34.33%	33.15%
	R	0.01	0.26	0.36	0.38
Station name	$PM_{2.5}$ in Jan,	SLAB	UCM	BEP	BEM
JQLH	MFB	−90.72%	39.00%	−25.05%	−34.34%
	MFE	52.29%	40.92%	30.23%	30.75%
	R	0.03	0.28	0.40	0.40
SLD	MFB	−130.86%	5.27%	−40.06%	−46.29%
	MFE	66.98%	45.38%	42.34%	41.85%
	R	0.05	0.27	0.23	0.23
LYS	MFB	−86.89%	10.29%	8.96%	5.15%
	MFE	49.35%	30.17%	30.71%	29.69%
	R	0.33	0.49	0.31	0.34
Overall	MFB	−102.82%	38.19%	−18.72%	−25.16%
	MFE	56.21%	38.82%	34.43%	34.10%
	R	0.14	0.35	0.31	0.32

Table 8
Statistical metrics for CMAQ model evaluation over Chengdu in July 2017.

Station name	NO_2 in July	SLAB	UCM	BEP	BEM
JQLH	MFB	−5.12%	52.47%	84.11%	49.07%
	MFE	38.12%	34.19%	46.95%	33.76%
	R	−0.19	0.37	0.49	0.30
SLD	MFB	−108.59%	−42.17%	−6.54%	−38.52%
	MFE	60.70%	39.10%	40.59%	37.80%
	R	−0.06	0.33	0.42	0.45
LYS	MFB	−37.30%	66.52%	71.52%	69.08%
	MFE	38.37%	43.98%	46.30%	45.31%
	R	0.09	0.12	0.18	0.06
Overall	MFB	−50.34%	25.61%	49.70%	26.54%
	MFE	45.73%	39.09%	44.61%	38.96%
	R	−0.05	0.27	0.36	0.27
Station name	$PM_{2.5}$ in July January	SLAB	UCM	BEP	BEM
JQLH	MFB	−38.81%	44.49%	77.92%	34.67%
	MFE	40.58%	39.86%	52.47%	36.74%
	R	0.16	0.41	0.29	0.33
SLD	MFB	−94.58%	−8.01%	25.32%	−8.47%
	MFE	49.86%	35.50	43.72%	34.31%
	R	0.01	0.48	0.46	0.31
LYS	MFB	64.03%	20.62%	30.26%	19.78%
	MFE	39.83%	36.08%	37.68%	38.48%
	R	0.11	0.01	0.19	0.14
Overall	MFB	−23.12%	19.03%	44.50%	15.33%
	MFE	43.42%	37.15%	44.62%	36.51%
	R	0.09	0.30	0.31	0.26

surface layer depth of nearly 20 m. The physical and chemical parameterizations for the WRF-CMAQ model are listed in Table 1. We simulated the meteorological conditions and air quality in January and July 2017 as the representative months in winter and summer. The first 10 days were treated as spin-up time and were not analysed in this study. The initial and boundary conditions in the WRF simulation are obtained from the National Centers for Environmental Prediction (NCEP) final 0.25° × 0.25° reanalysis data. The initial and boundary conditions of CMAQ are generated from the default profiles in the CMAQ model, which represent a clean atmosphere. Anthropogenic emissions of air pollutants are based upon the Multiresolution Emission Inventory for China (MEIC) in 2017, which was developed by Tsinghua University with a grid resolution of 0.25° × 0.25°(Zheng et al., 2018). The land cover and land use data used in WRF are updated by using Moderate-resolution Imaging Spectroradiometer (MODIS) land use products. The hourly meteorological observations are acquired from the China National Meteorological Center. The air quality monitoring data are obtained from the China Environmental Monitoring Center.

2.2. Urban canopy models in WRF

The parameters of urban canopy schemes are summarized in Table 2, Table 3, and Table 4 (He et al., 2009). Each urban canopy model has unique features in representing the parameterizations in urban regions. The single-layer urban canopy model (UCM) was proposed as a complex urban canopy model with advanced features, including the representation of the geometric shape of the city by assuming a street of infinite length and considering the three-dimensional urban surface, including walls, roofs, and roads (Kusaka et al., 2001; Kusaka and Kimura, 2004). The multilayer canopy layer model (BEP, building effect parameterization) developed by Martilli et al. (2002) not only inherits the model characteristics of the UCM but also allows direct interactions between the buildings and the planetary boundary layer (PBL) (Ezber et al., 2007) and considers the vertical distribution of energy between the three-dimensional urban surface and the buildings in the entire canopy. In the BEM model, the urban canopy is treated as a multilayer model with a building energy model including anthropogenic heat due to air-conditioning systems. The detailed city structure is well represented in the BEM model. In brief, the urban canopy model is divided into a single-layer urban canopy model (UCM) and a multilayer urban canopy model (BEP and BEM). The difference between these two types of urban canopies lies mainly in the impact on the energy budget over urban areas. The single-layer urban canopy model treats the heat flux between buildings and buildings as a constant variable, while the multilayer urban canopy model stratifies heat fluxes according to building height.

2.3. Data processing method

2.3.1. Method for updating the underlying surface data

The WRF urban canopy model in this study requires three new types of urban surfaces: high-density urban surfaces, medium-density urban surfaces, and low-density urban surfaces. The default underlying surface data in WRF were constructed in 2000 and contain a single urban surface type. Compared to the MODIS data in 2017, we detect that there are differences between the MODIS land use in 2017 and the outdated land-use data of WRF in 2000. To capture the variability of land use and land cover changes in Chengdu, we integrated MODIS global 500 m land use data in 2017 to reclassify the urban surface through 3*3 window statistics. As shown in Fig. 2, each grid has an index for land use type, either urban surface or nonurban surface. First, the dominant land use type of the window is determined, which is the type with the highest proportion in the window. If the dominant land use type is the urban land surface, we further calculate the proportion of the urban land surface in the current window. If the proportion of urban land use is less than 50%, it is treated as a low-density urban surface, and if it is between 50% and 80%, it is classified as a medium-density urban surface. Other situations are considered a high-density urban surface. Fig. 3 shows that the classified urban land-use types in Chengdu with downtown Chengdu and densely populated districts and counties are clearly identified.

2.3.2. Allocation of anthropogenic emission inventory

In this study, we adopted the Inventory Spatial Allocate Tool (ISAT) developed by Wang et al. (2019) for allocating the MEIC emission inventory to the CMAQ model grids. The spatial surrogates for transportation sources, residential sources, agricultural sources, and industrial sources in the emission allocation are road networks, population densities, land use types, and industrial points of interest (POIs), respectively. Fig. 4 presents the monthly average NO_x emission intensity in January and July 2017. The urban core area of Chengdu city exhibits the highest NO_x emission intensity, and NO_x emission hotspots are widely distributed in suburban regions and highways around the city.

2.3.3. Site description and measurement

In this study, observation data were used to verify the meteorological parameters and air pollutant concentrations simulated by WRF and CMAQ (Fig. 5). Hourly meteorological observations were obtained from four stations located in a different county of Chengdu: Chongzhou (CZ), Shuangliu (SL), Wenjiang (WJ), and Xindu (XD). All meteorological data are from the China Meteorological Data Service Center and have passed the rigorous quality check. Air pollutant concentrations simulated by the CMAQ model are validated by ambient measurements from JinQuanLiangHe (JQLH), ShiLiDian (SLD), and LingYanSi (LYS) stations. Among them, JQLH and SLD are located in the high-density and medium-low-density urban areas of Chengdu. LYS is a typical suburban site. In addition, the JQLH station is located in the Jinniu District of Chengdu, 50 m from the nearest road, and it is located in residential communities, while the SLD station is located in the Chenghua District of Chengdu, near the railway and road. The LYS site is a typical rural station located in Dujiangyan, Chengdu.

The statistical metrics applied in this study include the root mean square error (RMSE, Eq. (1)), mean bias (MB, Eq. (2)), and correlation coefficient (R, Eq. (3)). CMAQ statistical metrics are based on Boylan's recommendations (Boylan and Russell, 2006) using the mean fractional bias (MFB, Eq. (4)) and the mean fractional error (MFE, Eq. (5)) as

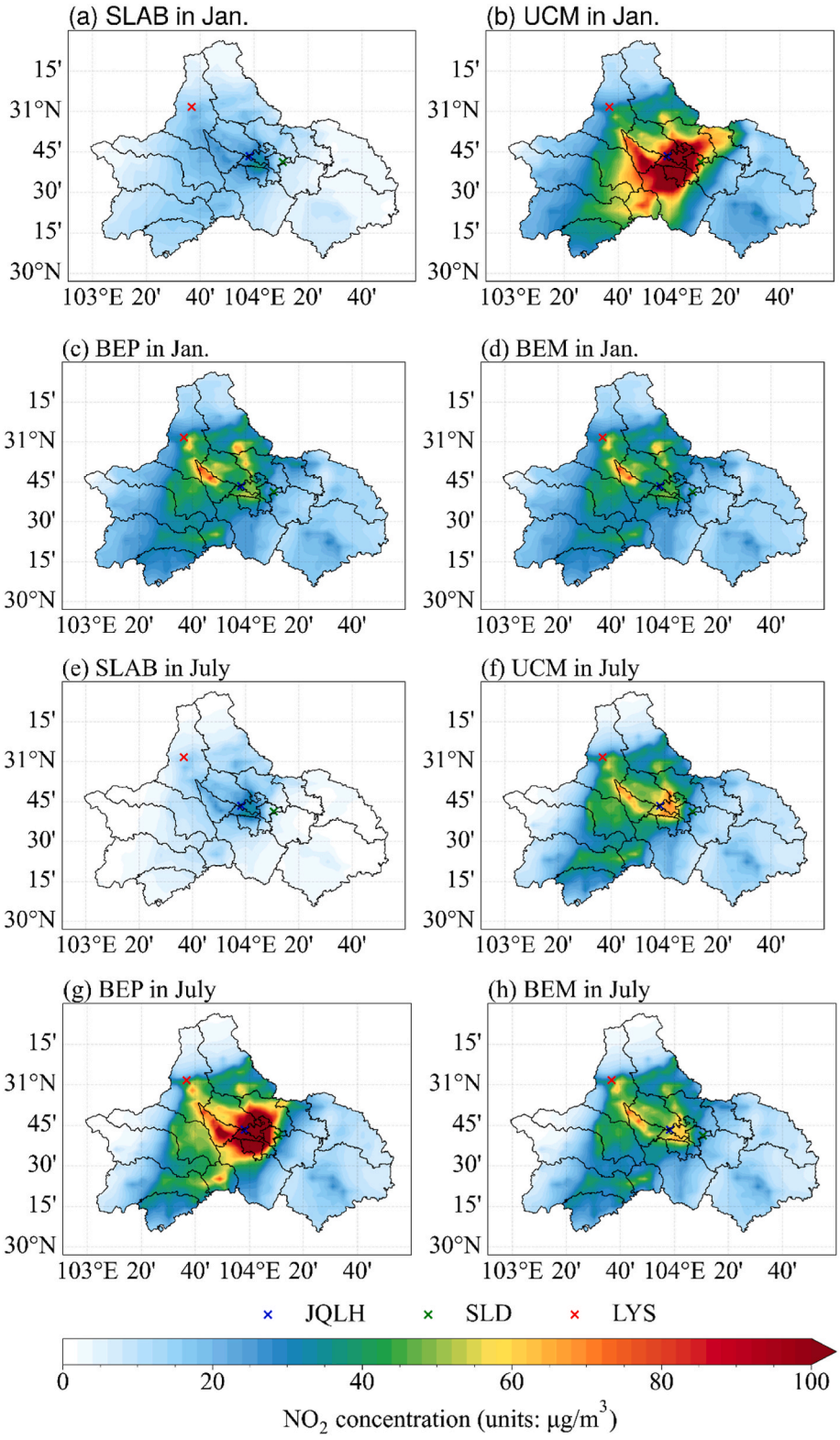

Fig. 8. Spatial distribution of ground-level NO_2 concentrations.

indicators to evaluate the robustness of the air quality model. If the MFB value is between −60% and 60% and the MFE is less than 75%, the model simulation result is considered to be within an acceptable range. The model performed well when meeting the criteria of an MFB value between −30% and 30% and an MFE less than 50%.

$$RMSE = \sqrt{\frac{1}{n}\sum_{i=1}^{n}(M_i - O_i)^2} \quad \text{Eq. 1}$$

$$MB = \frac{1}{n}\sum_{i=1}^{n}\left|M_i - O_i\right| \quad \text{Eq. 2}$$

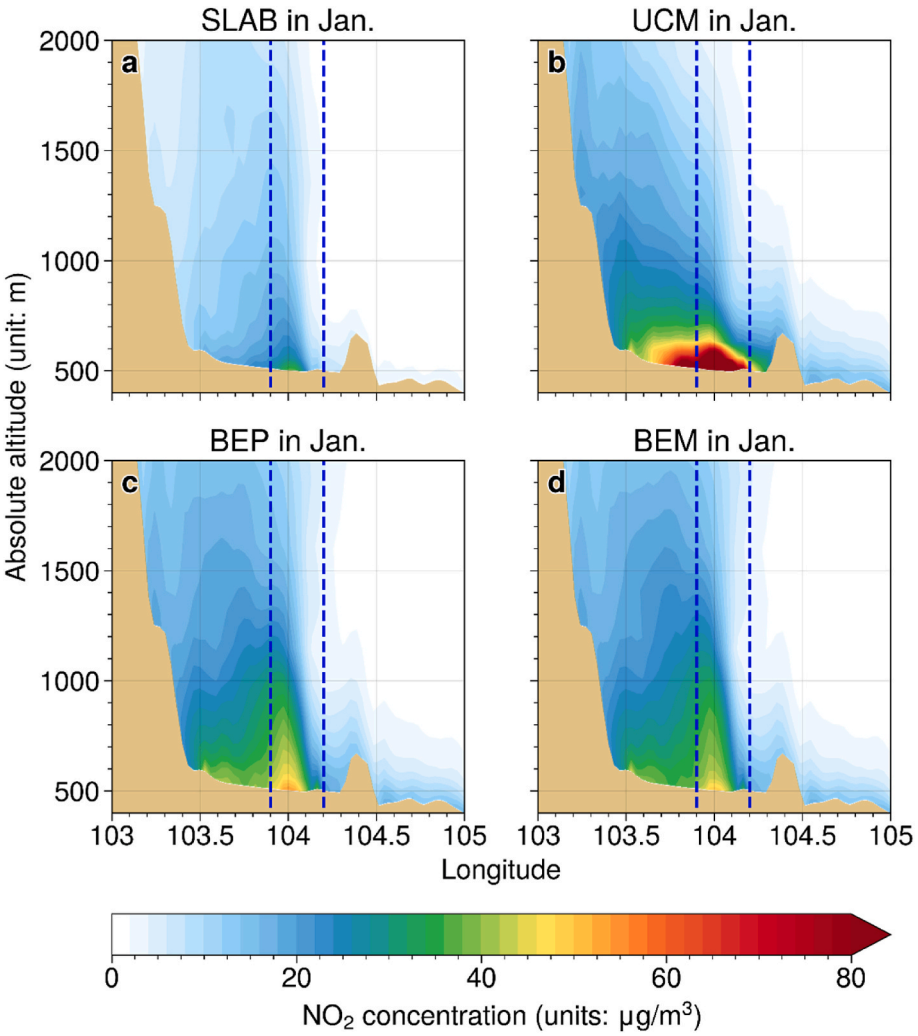

Fig. 9. Cross section of modelled NO_2 in January; (a)–(d) are the results of the SLAB, UCM, BEP and BEM models, respectively. Between the blue dotted lines is the downtown Chengdu. (For interpretation of the references to colour in this figure legend, the reader is referred to the Web version of this article.)

$$R = \frac{\sum_{i=1}^{n}\left(M_i - \overline{M}_i\right)\left(O_i - \overline{O}_i\right)}{\sqrt{\sum_{i=1}^{n}\left(M_i - \overline{M}_i\right)^2 \sum_{i=1}^{n}\left(O_i - \overline{O}_i\right)^2}} \quad \text{Eq. 3}$$

$$MFE = \frac{2}{n}\sum\left\{\frac{|M_i - O_i|}{(M_i + O_i)}\right\} \quad \text{Eq. 4}$$

$$MFB = \frac{2}{n}\sum\left\{\frac{(M_i - O_i)}{(M_i + O_i)}\right\} \quad \text{Eq. 5}$$

In the above formulas, n is the number of effective samples, and O_i and M_i denote the i-th observation value and the i-th simulated value, respectively. $\overline{O}$ and $\overline{M}$ represent the mean value of observations and simulated parameters, respectively.

3. Evaluation of model performance

3.1. Verification of meteorological conditions simulated by WRF

Fig. 6 and Fig. 7 show the diurnal patterns of the 2-m temperature at each site in January and July, respectively. Compared with observations, the UCM model tended to simulate a lower 2-m temperature than the SLAB model simulation of approximately −2.0 °C during January. The BEP and BEM models calculated higher 2-m temperatures than the SLAB model simulation of approximately 0.7 °C during 00:00–15:00 and 20:00–23:00 in January. The BEP and BEM models have a similar performance during 00:00–12:00 and 16:00–23:00, and the other times have a bias of −0.5 °C in January. For July, all the models simulated higher 2-m temperatures than the observation data during 09:00–19:00. While the BEP and BEM models have lower 2-m temperature during 00:00–08:00 and 20:00–23:00 with a bias of −0.5 °C, the statistical metrics suggest that the BEP and BEM with MBs of 1.76 °C and 2.04 °C, respectively and this is because of the higher prediction of the BEP and BEM models during 08:00–20:00. Overall, although the BEP and BEM models have similar performances, the BEP model simulation is lower than the BEM models.

Table 5 presents the statistical metrics of 2-m temperature under different urban canopy models. The SLAB model yields the best performance in January, with an MB value equal to 2.02 °C, while the UCM model performance is relatively weak in January, with an MB of 2.66 °C. Unlike wintertime, the UCM model performs well in the summer season with an MB of 1.73 °C. In contrast, the largest bias is found on the SLAB model with an MB value of 2.30 °C. While bias still existed among all models, the variations in observed temperature were well captured by all models with relatively low MB values, indicating the strong capability of the WRF model in reproducing 2-m temperature in Chengdu city.

Figs. S1–S8 show the verification of the 10-m wind fields at various sites in January and July. All model performances of the 10-m wind

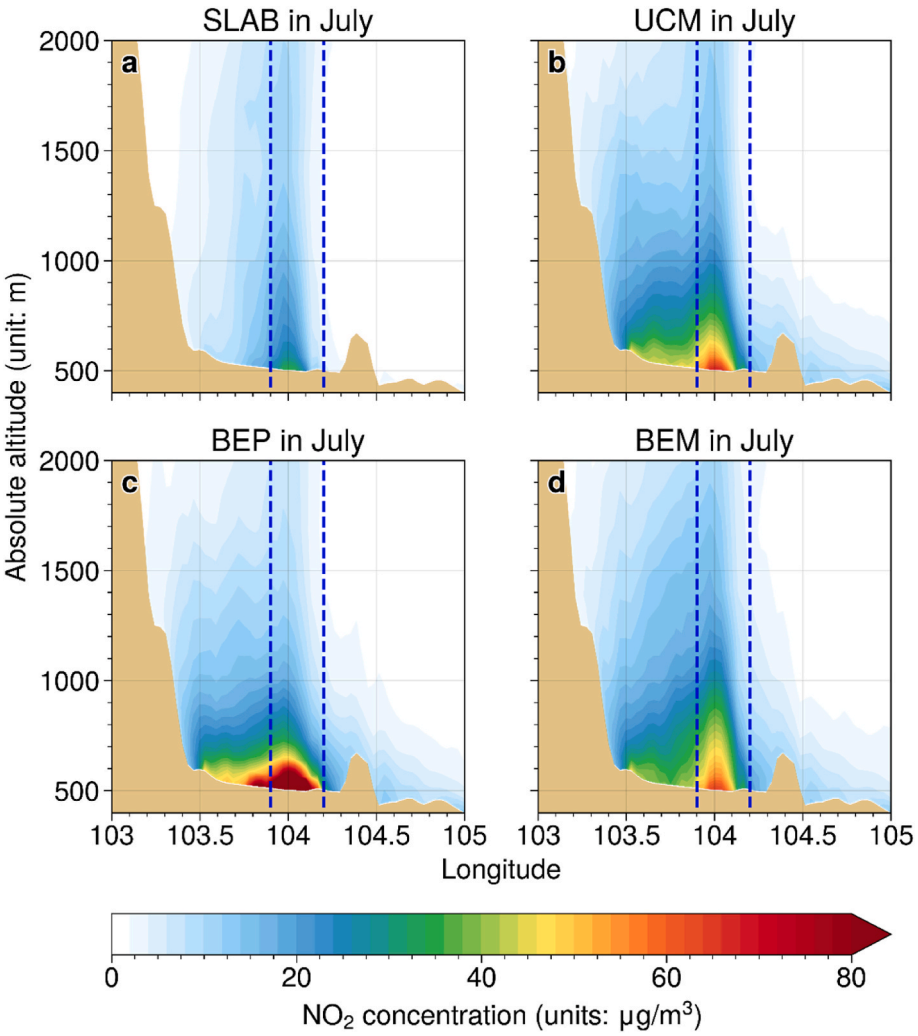

Fig. 10. Cross section of modelled NO_2 in July; (a)–(d) are the results of the SLAB, UCM, BEP and BEM models, respectively. Between the blue dotted lines is the downtown Chengdu. (For interpretation of the references to colour in this figure legend, the reader is referred to the Web version of this article.)

speed with MB less than 2.0 m/s in both winter and summer. In July, the MB was higher than that in January, and the overestimation of wind speed existed among all models. Similar to January, the 10-m wind speeds calculated by the BEP and BEM models are lower than those of the SLAB model and correlate better with the observations. Table 6 compares the statistical metrics of 10-m wind speed in various urban canopy models. Notably, MB values in the BEP model are comparatively low, with 1.00 m/s in January and 1.24 m/s in July, indicating that the BEP model presents the best model performance among the four models. Conversely, the model capabilities of the UCM and SLAB models were relatively poor in January (MB of 1.35 m/s) and July (MB of 1.6 m/s), respectively. Overall, the variations in meteorological conditions are well captured by the WRF simulations even though the model performance varies slightly among different urban canopy models.

3.2. *Verification of air pollutant levels simulated by CMAQ*

With the incorporation of the urban canopy model, the thermal and dynamic conditions in urban areas substantially changed and subsequently affected air pollutant concentrations. We select NO_2 and $PM_{2.5}$ as the criteria for air pollutants to further investigate the impact of the urban canopy on air quality modelling. Figs. S9–S12 depict the time series of NO_2 and $PM_{2.5}$ in January and July. Furthermore, the detailed statistical metrics for evaluating the CMAQ model performance in the winter and summer seasons are presented in Tables 7 and 8, respectively.

As shown in Fig. S9, NO_2 concentrations simulated under the SLAB model in urban areas (JQLH) and suburban areas (SLD) do not accurately capture the variability of NO_2 concentrations in winter. Specifically, the SLAB model performance for urban areas better fit the observed NO_2 levels, while the suburban areas do not reflect the real situation in terms of both trends and values with a bias of -20 μg/m^3. Meanwhile, the NO_2 concentrations simulated by the UCM model in winter show significant overestimations at all three sites, particularly in urban and suburban areas. Furthermore, the performance in winter for NO_2 concentrations is similar for the BEP and BEM models. Both urban and suburban areas can simulate realistic NO_2 concentrations well in winter, while rural areas (LYS) are somewhat overestimated.

As seen from Fig. S10, the SLAB model grossly underestimates $PM_{2.5}$ concentrations in urban and suburban areas in winter, while the $PM_{2.5}$ levels in rural areas are well represented. However, $PM_{2.5}$ concentrations in the UCM model were significantly overestimated by a factor of more than 2. Both the BEP and BEM models show occasional overestimations, and there are no obvious differences in modelled $PM_{2.5}$ concentrations between these models.

Fig. S11 and Fig. S12 show that the SLAB model underestimates both NO_2 and $PM_{2.5}$ concentrations in July. The UCM model performance of NO_2 and $PM_{2.5}$ concentrations are better in suburban areas in summer and has an overestimate in both rural and urban areas in summer. The BEP model suffers from an overestimation of both NO_2 and $PM_{2.5}$

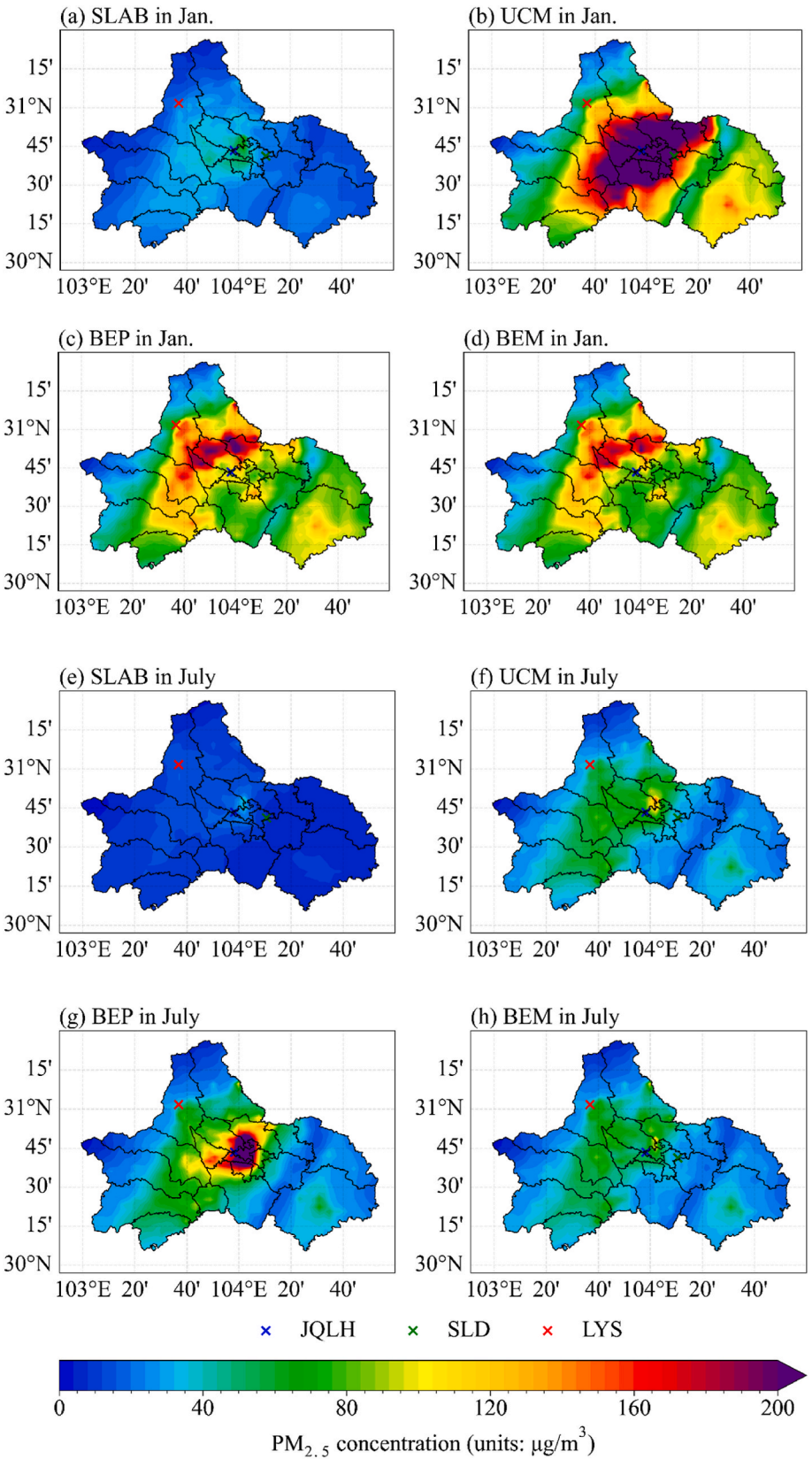

Fig. 11. Spatial distribution of ground-level $PM_{2.5}$ concentrations over Chengdu city in 2017.

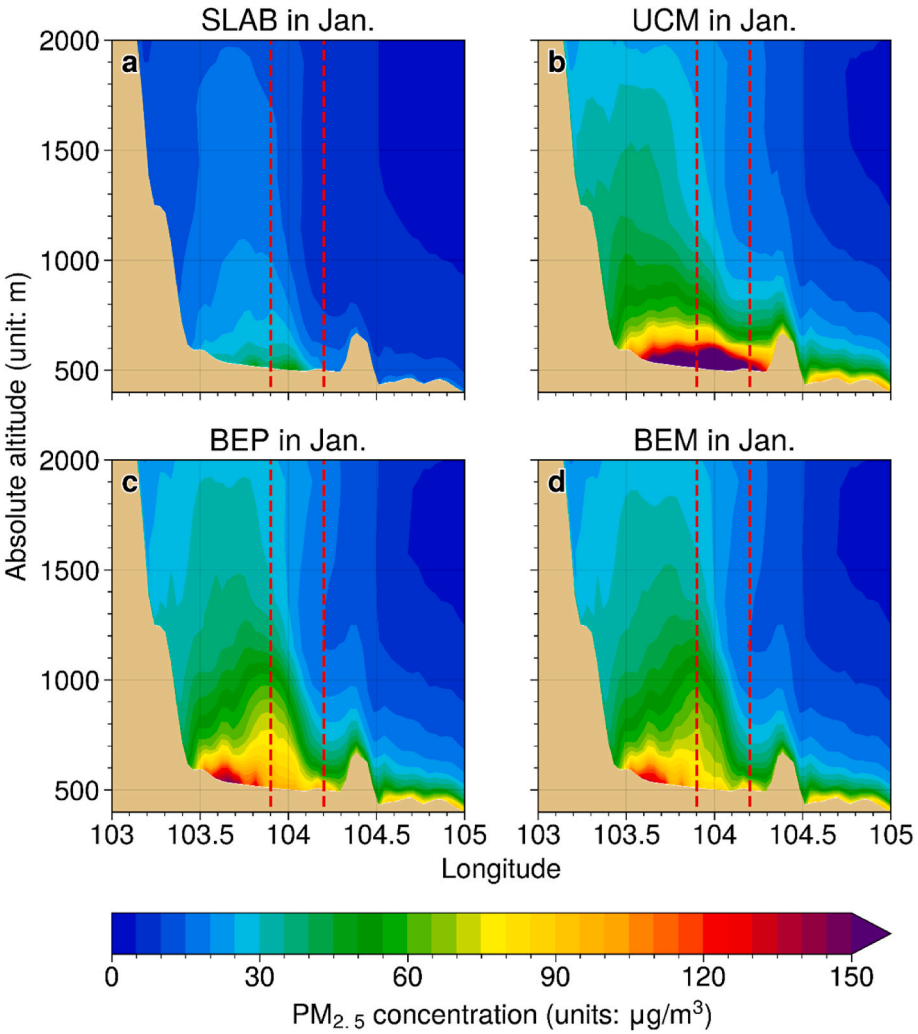

Fig. 12. Cross section of modelled $PM_{2.5}$ in January; (a)–(d) are the results of the SLAB, UCM, BEP and BEM models, respectively. Between the red dotted lines is the downtown Chengdu. (For interpretation of the references to colour in this figure legend, the reader is referred to the Web version of this article.)

concentrations in summer, particularly in urban and suburban areas, while it does not occur in the BEM model.

Table 7 illustrates that the SLAB model calculated the weakest NO_2 and $PM_{2.5}$ concentrations in winter, with MFBs (MFEs) of −52.93% (48.22%) and −102.82% (56.21%), respectively. The UCM model performs well in suburban areas for NO_2 concentrations in winter with an MFB (MFE) of 26.18% (38.32%) and is worse in rural areas with an MFB (MFE) of 62.58% (42.39%). The BEP model and BEM model simulations of NO_2 concentrations in winter perform better in urban and suburban areas but not in rural areas. For $PM_{2.5}$ concentrations, the SLAB model in winter performs poorly in urban, suburban, and rural areas, with R values of 0.03, 0.05, and 0.33, respectively. However, the performance in winter for $PM_{2.5}$ concentrations improved since we adopted the UCM, BEP, and BEM models with R values of 0.35, 0.31, and 0.32, respectively.

Table 8 illustrates that the SLAB model grossly underestimates NO_2 concentrations and does not reflect the true situation in terms of trends in summer. The UCM model for $PM_{2.5}$ concentrations performs very strongly in urban and suburban areas in summer with R values of 0.41 and 0.48, respectively, while it performs weakly in rural areas, mainly because it does not reflect the real situation in terms of trends. The BEP and BEM models are similar in terms of trend performance for both NO_2 and $PM_{2.5}$ concentrations, but there is a significant overestimate in the BEP model.

In general, the various models behave differently at different times. The SLAB model underestimates pollutant concentrations in both winter and summer. The UCM model is not suitable for modelling pollutants in winter, but the prediction of pollution concentrations is better in summer. The pollution concentrations calculated by the BEP model in winter are not significantly different from the prediction of the BEM model, but in summer, there is a significant overestimation of the BEP model.

4. Results and discussion

This section uses the results of the CMAQ model driven by different urban canopy models to examine the differences in the performance of NO_2 and $PM_{2.5}$ in different models in terms of spatial and vertical distributions.

4.1. NO_2 concentrations under different urban canopy models

Fig. 8 presents the spatial distributions of NO_2 in January and July 2017. The NO_2 concentrations simulated by the SLAB model are lower than those simulated by the other models in both January and July. In terms of spatial distribution, elevated NO_2 levels are concentrated in downtown Chengdu and along the highway. In July, the urban region of Chengdu city maintained high levels of NO_2 in the BEP model, while the NO_2 concentrations simulated by the BEM model were relatively low in July. For the UCM model, there are NO_2 hotspots over urban core regions in January, while this situation does not occur in July.

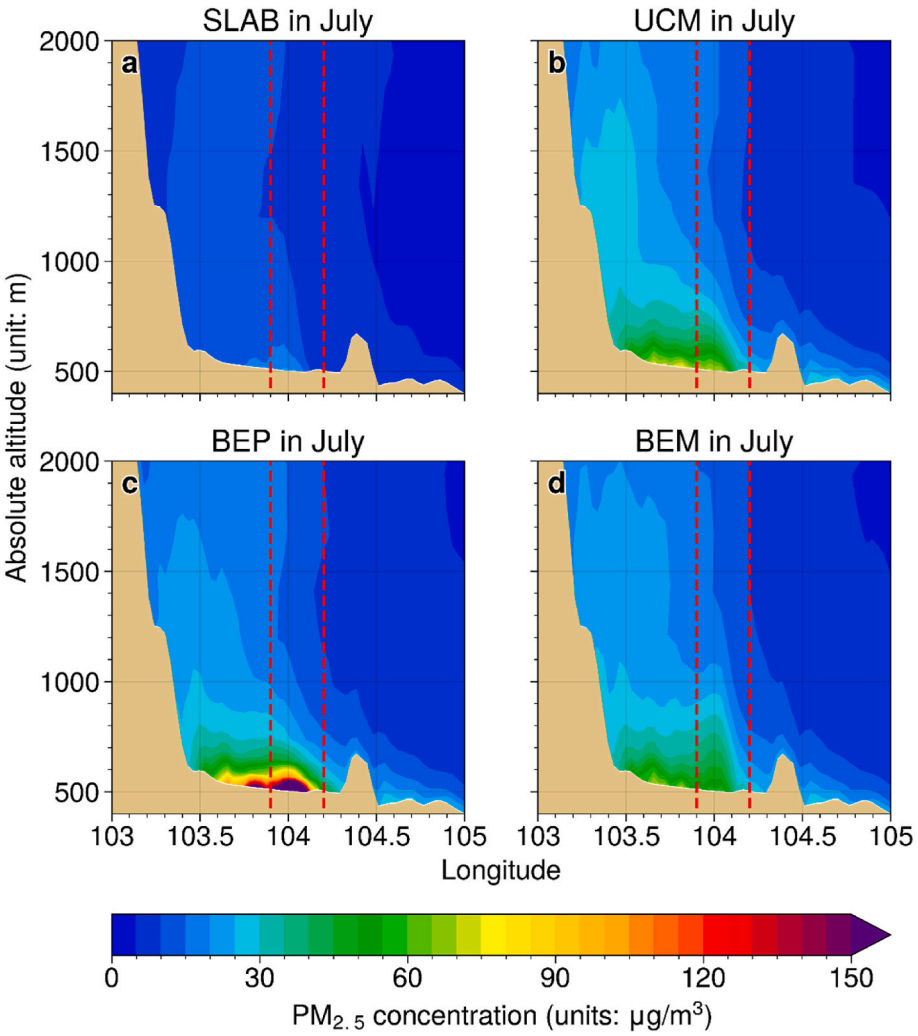

Fig. 13. Cross section of modelled $PM_{2.5}$ in July; (a)–(d) are the results of the SLAB, UCM, BEP and BEM models, respectively. Between the red dotted lines is the downtown Chengdu. (For interpretation of the references to colour in this figure legend, the reader is referred to the Web version of this article.)

Fig. 9 and Fig. 10 depict the cross-section of modelled NO_2 concentrations by each of the urban canopy models within WRF over Chengdu. Note that the cross-section of modelled air pollutants started at 103.0°E, 30.72°N and ended at 105.0°E, 30.72°N. The SLAB model predicted much lower pollutant concentrations than other urban canopy models in both January and July. Specifically, the maximum NO_2 concentrations simulated by the SLAB model in the Chengdu metropolitan area are 28 μg/m^3 in January and 26 μg/m^3 in July. In contrast, the urban region maintained a high level of NO_2 in January in the UCM model with surface concentrations exceeding 80 μg/m^3, while in July, the UCM model implied that NO_2 was dispersed, with maximum concentrations of approximately 60 μg/m^3. The modelled NO_2 levels are similar in magnitude between the BEP and BEM models in January, while the BEP model predicts much higher NO_2 concentrations in urban regions, suggesting that stagnant conditions over Chengdu city in summer may be well captured by the BEP model (Yang et al., 2020b).

4.2. *p.m.$_{2.5}$ concentrations under different urban canopy models*

Fig. 11 presents the spatial distributions of the ground-level $PM_{2.5}$ concentrations in January and July 2017. Overall, the $PM_{2.5}$ concentrations in January were much higher than those in July, and the comparison indicated that the simulated $PM_{2.5}$ concentrations in the UCM, BEP, and BEM models were higher than those in the SLAB model. In January, little difference exists between the BEP and BEM models. However, there are relatively large differences in the BEP and BEM models in July. This result is mainly attributed to the impact of air conditioning systems in the BEM model on the meteorological conditions that cause the BEP model to predict $PM_{2.5}$ hotspots over urban core regions, while elevated $PM_{2.5}$ concentrations are not presented in the BEM model. The UCM model suggests that the urban region of Chengdu city maintained high levels of $PM_{2.5}$ that were difficult to disperse, whereas this did not occur in July. This is due to the low elevation angle in winter when less solar radiation reaches the ground, and the shadow effect is evident. In summer, the influence of the shadow effect is less pronounced because more solar radiation reaches the ground. In addition, the UCM model has the lowest sensible heat flux (SHX) of 35 W/m^2 over the core region of Chengdu, while the SHX values in the SLAB, BEP, and BEM models are 65 W/m^2, 115 W/m^2, and 115 W/m^2 over the core region of Chengdu, respectively. In summer, the SLAB, UCM, BEP, and BEM models have sensible heat fluxes of 150 W/m^2, 125 W/m^2, 115 W/m^2, and 200 W/m^2 over the core region of Chengdu. Due to the much lower difference in SHX between the UCM model and other models in summer than in winter. Thus, the PBLH of the UCM model is significantly lower in winter (as shown in Fig. S17 and Fig. S18). Eventually, the UCM model causes $PM_{2.5}$ to have worse vertical mixing within the PBL in winter than in summer.

Fig. 12 and Fig. 13 present the cross-sections of the simulated $PM_{2.5}$ concentrations from different models in January and July, respectively. The $PM_{2.5}$ pollution in January is much more severe than that in July

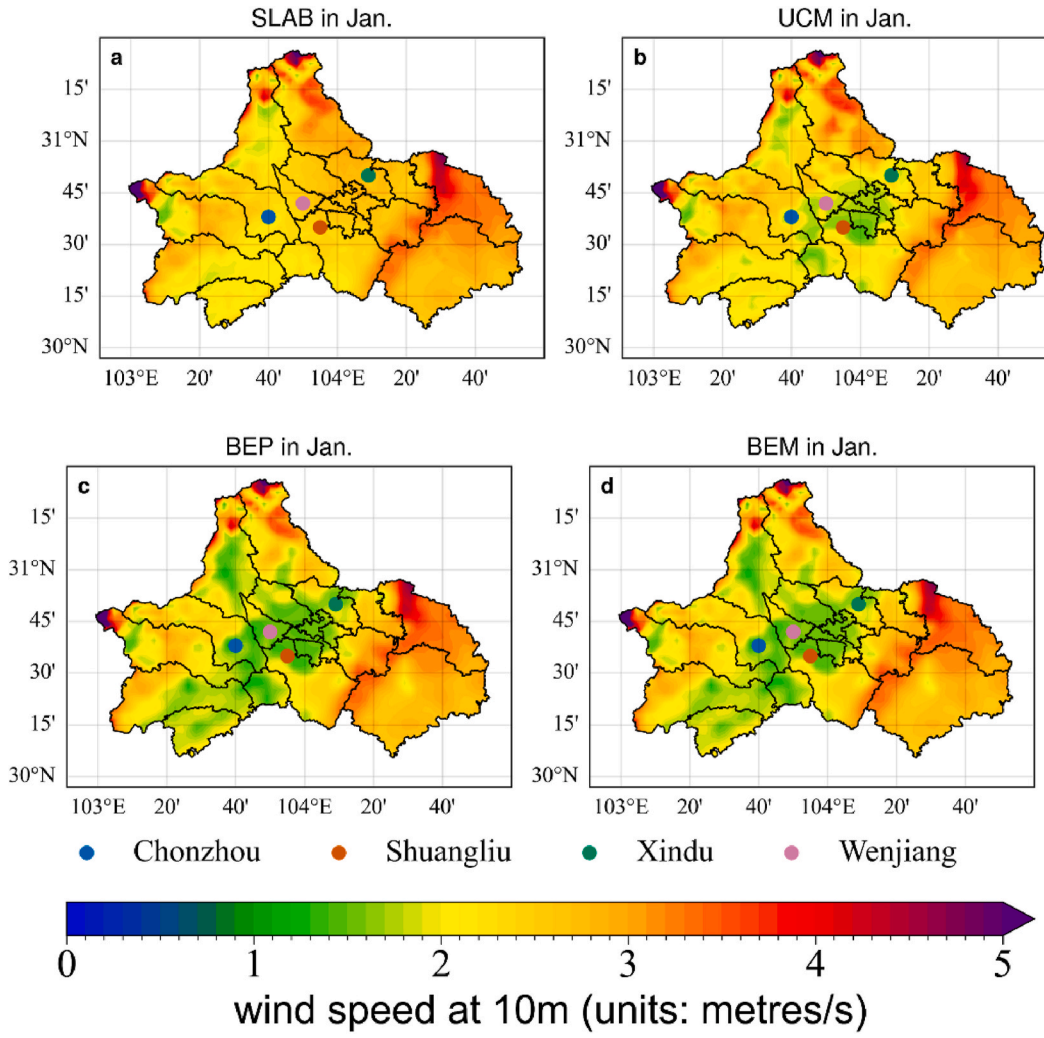

Fig. 14. Wind fields over Chengdu city under different urban canopy models in January 2017.

due to unfavourable meteorological conditions in wintertime (frequent stagnant conditions, persistent high relative humidity, poor ventilation, etc.) (Yang et al., 2020a; Wu et al., 2021). Moreover, it is worth noting that the $PM_{2.5}$ levels in the UCM, BEP, and BEM models are higher than those in the SLAB model regardless of the season. In July, the urban region of Chengdu maintained high levels of $PM_{2.5}$ of 150 $\mu g/m^3$ in the BEP model, while the BEM model predicted moderate $PM_{2.5}$ levels of 60 $\mu g/m^3$ over the urban core regions. In January, there are $PM_{2.5}$ hotspots over the urban core region in the UCM model, while the UCM model has favourable meteorological conditions for pollution diffusion in July.

4.3. Mechanistic exploration of varied model performance in urban canopy models

The differences between the various urban canopy models identified in the previous sections can be summarized as follows: 1) the SLAB model produces much lower pollutant concentrations than the other models; 2) the UCM model predicts elevated levels of air pollutants over the urban core region of Chengdu city in the summer, while simulated air pollutant concentrations in winter are relatively low; 3) the urban region of Chengdu city maintains high levels of air pollutants in the BEP model in July, while the BEM model considers that there are no pollution hotspots over the core region of Chengdu city. In this section, we further explore the mechanistic explanation of varied model performance in urban canopy models over Chengdu city. Note that the cross-section of modelled fields started at 103.0°E, 30.72°N and ended at 105.0°E, 30.72°N.

Fig. 14 and Fig. 15 present the horizontal fields of the 10-m wind speeds in January and July, respectively. The wind speed performance of the UCM model, the BEP model and the BEM model is less than that of the SLAB model on the urban surface in both January and July. This is because the UCM and BEP and BEM models take into account the three-dimensional structure of the city, which increases the surface roughness. Finally, the wind speed simulation results of these three models are smaller than those of the SLAB model. Due to the impacts of 10-m wind speeds, when the UCM, BEP, and BEM models simulate pollutants, the diffusion conditions are worse than those of the SLAB model. This ultimately leads to much lower pollutant concentrations near the ground in the SLAB model than those in other models. Despite the high PBLH of the SLAB model (Fig. S17 and Fig. S18), fewer pollutants are able to diffuse from the near surface to the upper layers, thus causing the SLAB model for pollution concentrations to differ significantly from other models in the vertical layer.

Fig. 16 and Fig. 17 illustrate the vertical temperature fields in January and July, respectively. From Fig. 17, it can be seen that the temperature near the ground calculated by the BEP model in July was significantly lower than that calculated by the BEM model. This is because, in summer, the air-conditioning system of the BEM model transfers indoor heat to the outside, which causes the increase of SHX on the ground compared to other models and the increment can be as great as 120 W/m^2 compared to BEP models which do not consider air conditioning systems (Fig. S16). This condition ultimately releases much

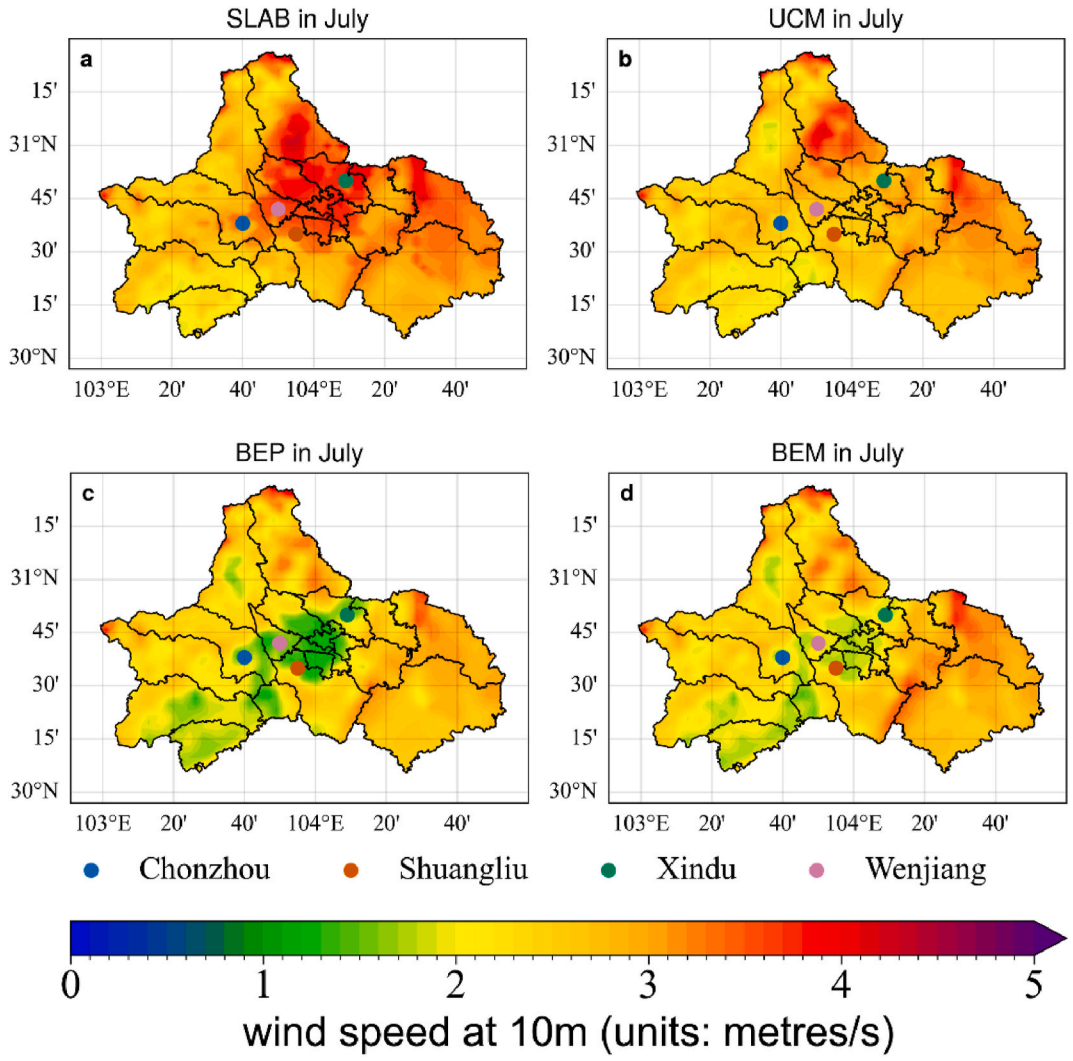

Fig. 15. Wind fields over Chengdu city under different urban canopy models in July 2017.

heat in the urban area and further leads to an increase in the surface temperature over the urban region of Chengdu. Such an increase in temperature may perturb and even substantially enhance the horizontal turbulence effect. As shown in Fig. 15(c) and (d), the prediction of 10-m wind speeds in the BEM model is higher than that in the BEP model. In addition, the increase in PBLH is due to the increase in temperature. Fig. S18 shows that the average PBLH over time simulated in the BEP model over the core region of Chengdu is 800 m, while it is 1100 m in the BEM model. A higher PBLH is generally conducive to the dispersion of air pollutants and dilutes atmospheric composition into a deep PBL. Thus, the ventilation condition in the BEM model may be better than that in the BEP model. The BEP model and the BEM model have similar simulations of near-surface temperature in January. This is largely caused by the low utilization rate of air conditioning in winter; thus, the air conditioning system in the BEM model shows minor impacts on the SHX (Fig. S15) and the external temperature.

The radiation budget in urban areas is modulated by the urban canopy environment, especially the effects of buildings within the city, namely, the shadow effect (SE) (Liao et al., 2014; Li et al., 2019). The SE is explained by low solar zenith angle in winter leading to less amount of solar radiation reaching the ground and subsequently result in less radiation shaded by the buildings while the high solar zenith angle in summer causing much solar radiation reaching the ground and a large portion of it blocked by buildings. The impacts of SE are the key reason for the UCM model. The low solar angle in winter means that less solar radiation reaches the ground and SE has a significant effect on temperature. Although the UCM model has AH, the corresponding effect is not sufficient to offset the SE. Meanwhile, the BEP and BEM models have higher surface albedo than the UCM model in both winter and summer seasons (Fig. S13 and Fig. S14), which can lead these to obtain stronger thermal inertia. Therefore, the BEP and BEM models will cool down slowly, and their AHs are sufficient to offset the SE. This phenomenon then results in the planetary boundary layer height (PBLH) simulated in the UCM model being lower than the BEP and BEM models in winter. In July, SE shows minor effects because of the high solar angle and intense radiation; thus, it does not drastically affect the modelled parameters in the UCM model.

5. Conclusion

In this study, the applicability of four urban canopy models incorporated in the WRF model and the impacts of these canopy models on the meteorological phenomenon and air quality are assessed by using the WRF–CMAQ modelling system. We evaluated the model performance of the four models in winter and summer against observations and explored the reasons for the differences in the models in winter and summer. The results show that the SLAB model underestimates pollutant concentrations in both winter and summer with MFBs of −50.34% and −23.12%, respectively. This can be attributed to the SLAB model not reflecting the real city form. The UCM model yields good performance,

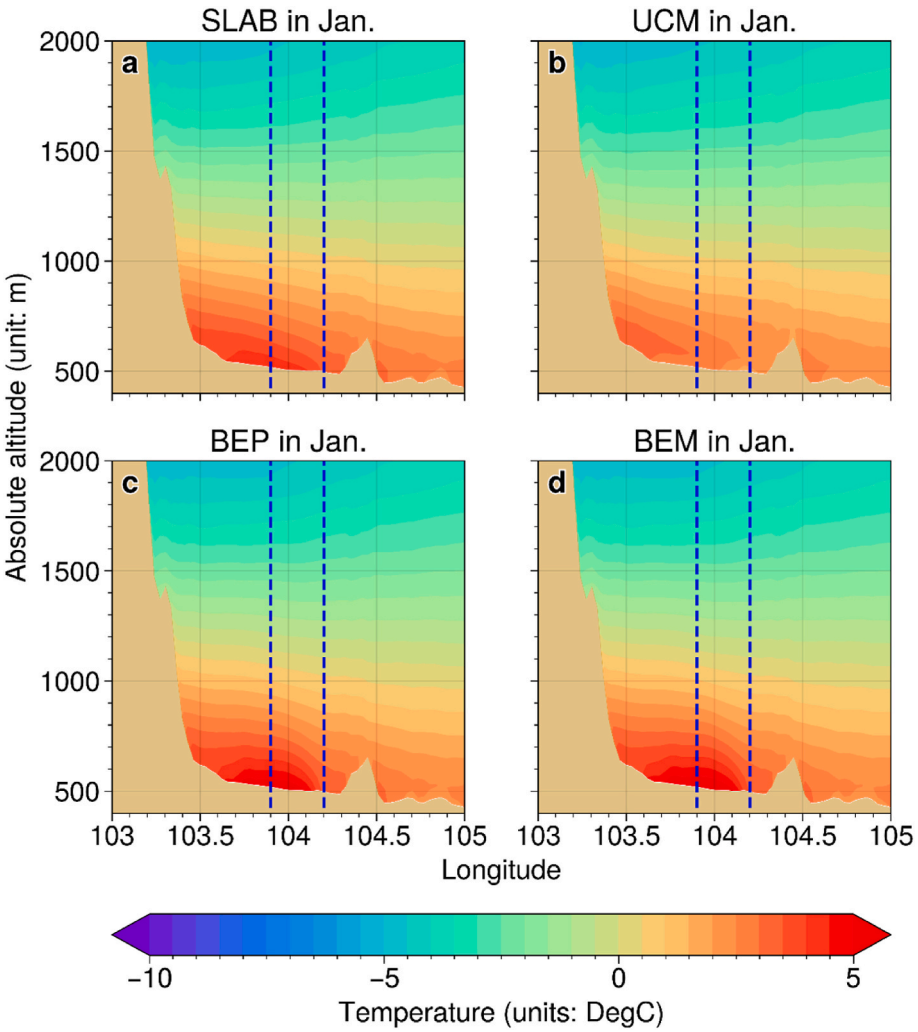

Fig. 16. Cross section of modelled temperature in January; (a)–(d) are the results of the SLAB, UCM, BEP and BEM models, respectively. Between the blue dotted lines is the downtown Chengdu. (For interpretation of the references to colour in this figure legend, the reader is referred to the Web version of this article.)

with MFBs (MFEs) of 25.61% (39.09%) and 19.03% (37.15%) in winter and summer, respectively. The BEP model is worse than the UCM model, with MFBs (MFEs) of 49.70% (44.61%) and 44.50% (44.62%) in winter and summer, respectively. Rather, the BEP model performs better than the UCM model in terms of a trend with R values of 0.36 and 0.31, respectively. The BEM models perform well in urban and suburban areas, with R values of 0.30 and 0.40 in winter and 0.33 and 0.31 in summer, respectively. All models do not perform well in rural areas. This can be attributed to allocation bias in the emission inventory and a lack of consideration of regional transport since the simulation domain only covered Chengdu city.

The main differences in model results due to model performance in this study are as follows: 1) the SLAB model underestimates pollutant concentrations in both winter and summer; 2) the UCM model overestimates pollutant concentrations in winter; and 3) the BEP model overestimates pollutant concentrations in summer. For the first case, the main reason is that the SLAB does not consider the urban canopy structure, resulting in lower surface roughness and less obstruction to wind speed, leading to overestimation in wind speed. Moreover, the SLAB model is better ventilated, as there is no canopy to shade the solar radiation, resulting in higher temperatures and higher PBLH in the SLAB model. In the second case, the shading effect is more pronounced in winter because the solar angle is low and less solar radiation reaches the ground. In contrast, the shading effect is not as pronounced in summer because the solar angle is high and most of the ground heat is provided by solar radiation in summer. The shading effect of the UCM model is, therefore, more pronounced in winter, resulting in lower surface temperature and decreased PBLH. The last case is mainly due to the higher thermal inertia of the BEP model than the single urban canopy model, which allows the urban surface to warm at a slow rate, in turn leading to low temperature, low PBLH, and poor ventilation. The BEM model exhibits better ventilation, as the air conditioning system takes a large amount of the indoor temperature outside, offsetting the temperature difference due to thermal inertia.

This study highlights the impacts of urban canopy models in simulating meteorological conditions and air quality in the megacity Chengdu and suggests that employing suitable urban canopy models could improve the WRF-CMAQ model performance. While this study updated the land use and further classified the urban land use category based on updated MODIS data, the integrated urban canopy parameters are still limited. Moving forward, integrating much detailed urban land dataset such as World Urban Database and Access Portal Tools (WUDAPT) into WRF-CMAQ modelling system will assist in improving the understanding of urban meteorology-air quality studies. A deeper understanding of the urban canopy could not only optimize urban air quality predictions but also help to develop climate adoption policies.

CRediT authorship contribution statement

Haofan Wang: Conceptualization, Methodology, Formal analysis,

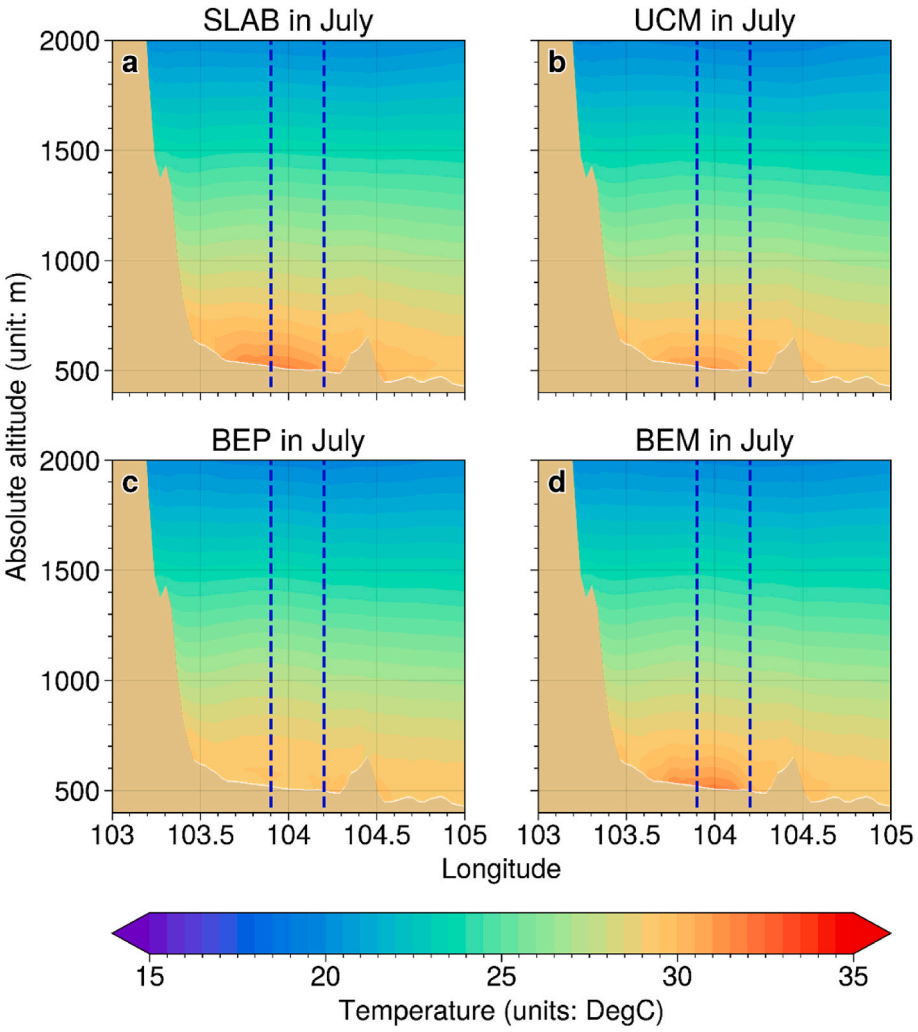

Fig. 17. Cross section of modelled temperature in July; (a)–(d) are the results of the SLAB, UCM, BEP and BEM models, respectively. Between the blue dotted lines is the downtown Chengdu. (For interpretation of the references to colour in this figure legend, the reader is referred to the Web version of this article.)

Investigation, Writing – original draft, Visualization, Project administration. **Zhihong Liu:** Conceptualization, Project administration. **Yang Zhang:** Conceptualization, Writing – review & editing, Project administration. **Zhengyang Yu:** Resources, Data curation. **Chunrong Chen:** Resources, Data curation.

Declaration of competing interest

The authors declare that they have no known competing financial interests or personal relationships that could have appeared to influence the work reported in this paper.

Acknowledgements

This study was funded by the National Natural Science Foundation of China (No. 41771535), the Scientific Research Foundation of CUIT (No. KYTZ201909) and the Science and Technology Department of Sichuan Province Foundation (No. 21YYJC3604). The authors thank the MEIC team from Tsinghua University for providing the Multiscale Emission Inventory of China (MEIC). The authors acknowledge helpful discussions with Jiaxin Qiu from Jilin University.

Appendix A. Supplementary data

Supplementary data to this article can be found online at https://doi.org/10.1016/j.atmosenv.2021.118775.

References

Arnfield, A.J., 2003. Two decades of urban climate research: a review of turbulence, exchanges of energy and water, and the urban heat island. Int. J. Climatol. 23, 1–26. https://doi.org/10.1002/joc.859.

Barlow, J.F., 2014. Progress in observing and modelling the urban boundary layer. Urban Climate 10, 216–240. https://doi.org/10.1016/j.uclim.2014.03.011.

Boylan, J.W., Russell, A.G., 2006. PM and light extinction model performance metrics, goals, and criteria for three-dimensional air quality models. Atmos. Environ. 40, 4946–4959. https://doi.org/10.1016/j.atmosenv.2005.09.087.

Chen, S.-H., Sun, W.-Y., 2002. A one-dimensional time dependent cloud model. J. Meteorol. Soc. Japan Ser II 80, 99–118.

Chou, M.-D., Suarez, M.J., Liang, X.-Z., et al., 2001. A Thermal Infrared Radiation Parameterization for Atmospheric Studies.

Ek, M.B., Mitchell, K.E., Lin, Y., et al., 2003. Implementation of Noah land surface model advances in the National Centers for Environmental Prediction operational mesoscale Eta model. J. Geophys. Res. 108 https://doi.org/10.1029/2002JD003296, 2002JD003296.

Ezber, Y., Lutfi Sen, O., Kindap, T., Karaca, M., 2007. Climatic effects of urbanization in istanbul: a statistical and modeling analysis. Int. J. Climatol. 27, 667–679. https://doi.org/10.1002/joc.1420.

Gu, S., Guenther, A., Faiola, C., 2021. Effects of anthropogenic and biogenic volatile organic compounds on Los Angeles air quality. Environ. Sci. Technol. https://doi.org/10.1021/acs.est.1c01481.

He, X., Jiang, W., Zhou, R., 2009. Development of a single-layer urban canopy model and numerical experiments. Chin. J. Atmos. Sci. 33, 981–993.

Hu, C., Kang, P., Jaffe, D.A., et al., 2021. Understanding the impact of meteorology on ozone in 334 cities of China. Atmos. Environ. 248, 118221. https://doi.org/10.1016/j.atmosenv.2021.118221.

Janjić, Z.I., 1994. The step-mountain eta coordinate model: further developments of the convection, viscous sublayer, and turbulence closure schemes. Mon. Weather Rev. 122, 927–945.
Kusaka, H., Kimura, F., 2004. Coupling a single-layer urban canopy model with a simple atmospheric model: impact on urban heat island simulation for an idealized case. J. Meteorol. Soc. Jpn. 82, 67–80. https://doi.org/10.2151/jmsj.82.67.
Kusaka, H., Kondo, H., Kikegawa, Y., Kimura, F., 2001. A simple single-layer urban canopy model for atmospheric models: comparison with multi-layer and slab models. Boundary-Layer Meteorol. 101, 329–358.
Li, M., Song, Y., Mao, Z., et al., 2016. Impacts of thermal circulations induced by urbanization on ozone formation in the Pearl River Delta region, China. Atmos. Environ. 127, 382–392. https://doi.org/10.1016/j.atmosenv.2015.10.075.
Li, Y., Zhang, J., Sailor, D.J., Ban-Weiss, G.A., 2019. Effects of urbanization on regional meteorology and air quality in Southern California. Atmos. Chem. Phys. 19, 4439–4457. https://doi.org/10.5194/acp-19-4439-2019.
Liao, J., Wang, T., Jiang, Z., et al., 2015. WRF/Chem modeling of the impacts of urban expansion on regional climate and air pollutants in Yangtze River Delta, China. Atmos. Environ. 106, 204–214. https://doi.org/10.1016/j.atmosenv.2015.01.059.
Liao, J., Wang, T., Wang, X., et al., 2014. Impacts of different urban canopy schemes in WRF/Chem on regional climate and air quality in Yangtze River Delta, China. Atmos. Res. 145 (146), 226–243. https://doi.org/10.1016/j.atmosres.2014.04.005.
Lin, C., Chen, W., Liu, S., et al., 2008. Numerical study of the impact of urbanization on the precipitation over Taiwan. Atmos. Environ. 42, 2934–2947. https://doi.org/10.1016/j.atmosenv.2007.12.054.
Ma, M., Gao, Y., Wang, Y., et al., 2019. Substantial ozone enhancement over the North China Plain from increased biogenic emissions due to heat waves and land cover in summer 2017. Atmos. Chem. Phys. 19, 12195–12207. https://doi.org/10.5194/acp-19-12195-2019.
Martilli, A., Clappier, A., Rotach, M.W., 2002. An urban surface exchange parameterisation for mesoscale models. Boundary-Layer Meteorol. 104, 261–304.
Memon, R.A., Leung, D.Y.C., Liu, C.-H., 2009. An investigation of urban heat island intensity (UHII) as an indicator of urban heating. Atmos. Res. 94, 491–500. https://doi.org/10.1016/j.atmosres.2009.07.006.
Mlawer, E.J., Taubman, S.J., Brown, P.D., et al., 1997. Radiative transfer for inhomogeneous atmospheres: RRTM, a validated correlated-k model for the longwave. J. Geophys. Res. 102, 16663–16682. https://doi.org/10.1029/97JD00237.
Murphy, B.N., Woody, M.C., Jimenez, J.L., et al., 2017. Semivolatile POA and parameterized total combustion SOA in CMAQv5.2: impacts on source strength and partitioning. Atmos. Chem. Phys. 17, 11107–11133. https://doi.org/10.5194/acp-17-11107-2017.
Pye, H.O.T., Murphy, B.N., Xu, L., et al., 2017. On the implications of aerosol liquid water and phase separation for organic aerosol mass. Atmos. Chem. Phys. 17, 343–369. https://doi.org/10.5194/acp-17-343-2017.
Salamanca, F., Martilli, A., Tewari, M., Chen, F., 2011. A study of the urban boundary layer using different urban parameterizations and high-resolution urban canopy parameters with WRF. J. Appl. Meteorol. Climatol. 50, 1107–1128. https://doi.org/10.1175/2010JAMC2538.1.
Skamarock, W.C., Klemp, J.B., Dudhia, J., et al., 2019. A Description of the Advanced Research WRF Model Version 4. UCAR/NCAR.
US EPA Office Of Research And Development, 2020. CMAQ. Version 5.3.2. Zenodo. https://zenodo.org/record/4081737.
Vahmani, P., Ban-Weiss, G.A., 2016. Impact of remotely sensed albedo and vegetation fraction on simulation of urban climate in WRF-urban canopy model: a case study of the urban heat island in Los Angeles. J. Geophys. Res. Atmos. 121, 1511–1531. https://doi.org/10.1002/2015JD023718.
Wang, H., Wu, K., Liu, Y., et al., 2021a. Role of heat wave-induced biogenic VOC enhancements in persistent ozone episodes formation in Pearl River Delta. J. Geophys. Res. Atmos. 126 https://doi.org/10.1029/2020JD034317.
Wang, K., Gao, C., Wang, C., et al., 2019. Research on emission inventory processing tool based on CSGD data. Res. Environ. Sci. 32, 1090–1098. https://doi.org/10.13198/j.issn.1001-6929.2019.02.13.
Wang, J., Hu, X.-M., 2020. Evaluating the performance of WRF urban schemes and PBL schemes over Dallas Fort Worth during a dry summer and a wet summer. J. Appl. Meteorol. Climatol. https://doi.org/10.1175/JAMC-D-19-0195.1.
Wang, K., Tong, Y., Gao, J., et al., 2021b. Impacts of LULC, FDDA, Topo-wind and UCM schemes on WRF-CMAQ over the Beijing-Tianjin-Hebei region, China. Atmospheric Poll. Res. 12, 292–304. https://doi.org/10.1016/j.apr.2020.11.011.
Wang, X., Chen, F., Wu, Z., et al., 2009. Impacts of weather conditions modified by urban expansion on surface ozone: comparison between the Pearl River Delta and Yangtze River Delta regions. Adv. Atmos. Sci. 26, 962–972.
Wu, K., Kang, P., Tie, X., et al., 2019. Evolution and assessment of the atmospheric composition in Hangzhou and its surrounding areas during the G20 summit. Aerosol Air Qual. Res. https://doi.org/10.4209/aaqr.2018.12.0481.
Wu, K., Yang, X., Chen, D., Gu, S., Lu, Y., Jiang, Q., et al., 2020. Estimation of biogenic VOC emissions and their corresponding impact on ozone and secondary organic aerosol formation in China. Atmos. Res. 231, 104656 https://doi.org/10.1016/j.atmosres.2019.104656.
Wu, K., Zhu, S., Liu, Y., et al., 2021. Modeling ammonia and its uptake by secondary organic aerosol over China. Geophys Res Atmos 126. https://doi.org/10.1029/2020JD034109.
Yan, D., Liu, T., Dong, W., et al., 2020. Integrating remote sensing data with WRF model for improved 2-m temperature and humidity simulations in China. Dynam. Atmos. Oceans 89, 101127. https://doi.org/10.1016/j.dynatmoce.2019.101127.
Yang, X., Lu, Y., Zhu, X., et al., 2020a. Formation and evolution mechanisms of severe Haze pollution in the Sichuan Basin, southwest China. Aerosol Air Qual Res 20, 2557–2567. https://doi.org/10.4209/aaqr.2020.04.0173.
Yang, X., Wu, K., Lu, Y., et al., 2021. Origin of regional springtime ozone episodes in the Sichuan Basin, China: role of synoptic forcing and regional transport. Environ. Pollut. 278, 116845. https://doi.org/10.1016/j.envpol.2021.116845.
Yang, X., Wu, K., Wang, H., et al., 2020b. Summertime ozone pollution in Sichuan Basin, China: meteorological conditions, sources and process analysis. Atmos. Environ. 226, 117392. https://doi.org/10.1016/j.atmosenv.2020.117392.
Yarwood, G., Jung, J., Whitten, G.Z., et al., 2010. Updates to the carbon Bond mechanism for version 6 (CB6). In: 9th Annual CMAS Conference. Chapel Hill, NC, pp. 11–13.
Zhang, H., Sato, N., Izumi, T., et al., 2008. Modified RAMS-urban canopy model for heat island simulation in chongqing, China. J. Appl. Meteorol. Climatol. 47, 509–524. https://doi.org/10.1175/2007JAMC1397.1.
Zhang, N., Gao, Z., Wang, X., Chen, Y., 2010. Modeling the impact of urbanization on the local and regional climate in Yangtze River Delta, China. Theor. Appl. Climatol. 102, 331–342. https://doi.org/10.1007/s00704-010-0263-1.
Zheng, B., Tong, D., Li, M., et al., 2018. Trends in China's anthropogenic emissions since 2010 as the consequence of clean air actions. Atmos. Chem. Phys. 18, 14095–14111. https://doi.org/10.5194/acp-18-14095-2018.
Zhu, K., Xie, M., Wang, T., et al., 2017. A modeling study on the effect of urban land surface forcing to regional meteorology and air quality over South China. Atmos. Environ. 152, 389–404. https://doi.org/10.1016/j.atmosenv.2016.12.053.